Fundamental and second-order phonon processes in CdTe and ZnTe

M. Schall, M. Walther, and P. Uhd Jepsen
Department of Molecular and Optical Physics, Fakultät für Physik, Albert-Ludwigs-Universität Freiburg, Hermann-Herder-Strasse 3, D-79104 Freiburg, Germany

(Received 1 March 2001; revised manuscript received 15 May 2001; published 3 August 2001)

Fundamental and higher-order photon-phonon interactions dominate the far infrared absorption and dispersion spectrum of most semiconductors and dielectrics. We present a detailed investigation of the temperature dependence of the dielectric function of the important II-VI semiconductors CdTe and ZnTe in the frequency range below 3 THz, between 10 and 300 K. From the dielectric function we determine the temperature dependence of the fundamental transverse-optical (TO) frequency in CdTe and ZnTe as well as the TO phonon damping rate in CdTe, and the dynamic ionic charge of both crystals is inferred from the measurements. Furthermore, our experimental data enable unambiguous assignment of low-frequency absorption bands to sum and difference combinations of fundamental phonon modes at critical points away from the Brillouin zone center.

DOI: 10.1103/PhysRevB.64.094301 PACS number(s): 78.30.Fs, 63.20.Kr

I. INTRODUCTION

Electro-optic crystals with ultrafast response time are of enormous technological and scientific importance. As an example, the introduction of electro-optic materials for detection of subpicosecond electrical transients (terahertz, or THz pulses)[1–3] has kicked-off new research directions which complement techniques based on photoconductive materials[4–6] for static spectroscopy in the far infrared. In combination with amplified femtosecond laser systems, the application of electro-optic materials offers the additional possibility of time-resolved THz spectroscopy,[7–10] hence allowing studies of ultrafast transient processes in the far infrared. Picosecond time-resolved THz spectroscopy has also been performed with photoconductive antennas.[11,12] In these experiments the optical-pump pulses were delivered by an unamplified fs oscillator, with natural limitations of pump energy and tunability compared to an amplified laser system.

It has turned out that for applications in the low part of the THz regime (<5 THz) ZnTe is the first choice as electro-optic detector of freely propagating THz pulses because of almost ideal properties when used in conjunction with pump-laser systems operating near 800 nm, and because of the availability of high-quality, low-price crystals from commercial suppliers. The useful spectroscopic range of ZnTe as emitter or detector is limited by the following factors. The frequency-dependent electro-optic susceptibility, absorption of the crystal represented by the absorption coefficient $\alpha(\nu)$, and mismatch between the group velocity of the optical-probe pulse and the phase velocity of the frequency components of the THz field.[13–15] The strong fundamental transverse-optical (TO) phonon resonance at 5.32 THz (at room temperature),[15] together with weaker combination bands at lower frequencies, results in strong dispersion in the frequency band below the TO resonance, and limits the detection bandwidth to below 3 THz in a 1-mm thick crystal. By application of thin emitter and detector crystals[13,16,17] and ultrashort (10 fs) optical-probe pulses it has recently become possible to perform spectroscopy above the TO frequency in the frequency band between 7 and 40 THz,[18] and ultrashort THz pulses were recently used in the direct observation of carrier dynamics on the 10-fs time scale.[19,20]

In this paper we present a measurement of the absorption- and dispersion spectra of CdTe and ZnTe below 3 THz, in the temperature range between 10 K and 300 K, with the goal of illuminating the importance of interactions between long-wavelength photons and vibrational modes of the crystal lattice in the interpretation of the spectra.

The paper is organized as follows. In the first section we discuss the experimental conditions and present experimental spectra of the absorption coefficient and index of refraction of the crystals.

The next section of the paper discusses spectral features originating from the fundamental TO resonance in the crystals. We demonstrate that with the measurement of both absorption and dispersion we can for the first time determine the temperature dependence of the TO resonance frequency in both CdTe and ZnTe, as well as the linewidth of the TO resonance in CdTe, even though the TO frequencies in both crystals lie outside of the spectral range of our spectrometer.

In the last part of the paper we present a detailed investigation of low-frequency phonon combination bands in ZnTe and CdTe below 3 THz. We use the temperature dependence of the absorption strengths in the temperature range from 10 K to 300 K to make the first unambiguous identification of the combination bands in ZnTe as a mixture of LO-LA (longitudinal-optical and -acoustical) differences at the *X* and *L* points of the Brillouin zone. We use CdTe, which possesses the well-understood 2TA(X) combination mode (the overtone of the transverse acoustic mode at the *X* point of the Brillouin zone) at 2.1 THz,[21,22] as reference case to verify the applicability of the method.

Differences between the absorption spectra at room temperature and cryogenic temperatures have previously been used to assist assignment of observed bands in CdTe[21,22] and ZnTe.[23] Only very recently the explicit temperature dependence has been used in the assignment of combination bands in $KTaO_3$.[24]

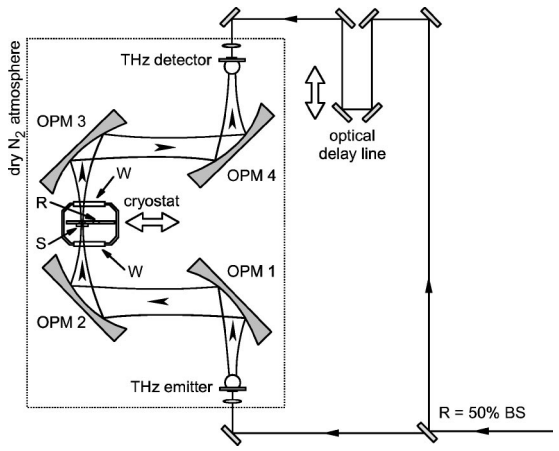

FIG. 1. Schematic of the experimental setup. Legend: OPM 1–4, off-axis paraboloidal mirrors; $f=120$ mm; R/S, reference/sample apertures in cryostat; BS, beam splitter.

II. EXPERIMENTAL SETUP

We measure the absorption and refractive-index spectra of the samples with a conventional terahertz time-domain spectrometer,[6] as illustrated in Fig. 1. Photoconductive dipole antennas, driven by 40 fs pulses from a mode-locked Ti:sapphire oscillator, are used to generate and detect the THz pulses, which consist of a single cycle of the electromagnetic field with subpicosecond duration. The resulting spectrum has a useful bandwidth from 0.1 to 3 THz. The emitter is fabricated on semi-insulating GaAs, and we use edge illumination of the positive electrode[25] for the generation of the strongest possible pulse. The detector is fabricated on a radiation-damaged silicon-on-sapphire substrate. The active area is 10 μm wide and 30 μm long.

The first-two off-axis paraboloidal mirrors (OPM 1 and OPM 2 in Fig. 1) in the THz beam path are used in a $f-2f-f$ geometry to focus the beam of THz pulses to a nearly frequency independent,[26] 1-mm spot size at an intermediate focus inside a cryostat where the sample and an identical reference aperture are mounted. OPM 3 and OPM 4 are used to image the intermediate focus onto the detector, again in a $f-2f-f$ geometry. The THz beam path is purged with dry nitrogen in order to avoid absorption induced by rotational transitions in water molecules.

A THz pulse propagating through the reference or sample aperture is in the following referred to as a *reference pulse* or *sample pulse*, characterized by the measured electric fields $E_r(t)$ and $E_s(t)$, respectively.

The dielectric function of the sample may be represented by the intensity absorption coefficient $\alpha(\nu)$ and the refractive index $n(\nu)$, and is calculated at each frequency ν within the bandwidth of the pulses from the ratio $R(\nu)=E_s(\nu)/E_r(\nu)=A(\nu)\exp[i\Delta\phi(\nu)]$ of the Fourier transforms of the sample pulse and the reference pulse. The refractive index is determined by the phase of R as $n=1+c\Delta\phi/2\pi\nu d$, and the absorption coefficient is calculated from the amplitude of R as $\alpha=-2\ln[A(n+1)^2/4n]/d$, where d is the thickness of the sample. This simple analysis assumes that the absorption is so low that the phase-shift associated with the transmission over the dielectric interfaces of the crystals can be neglected.

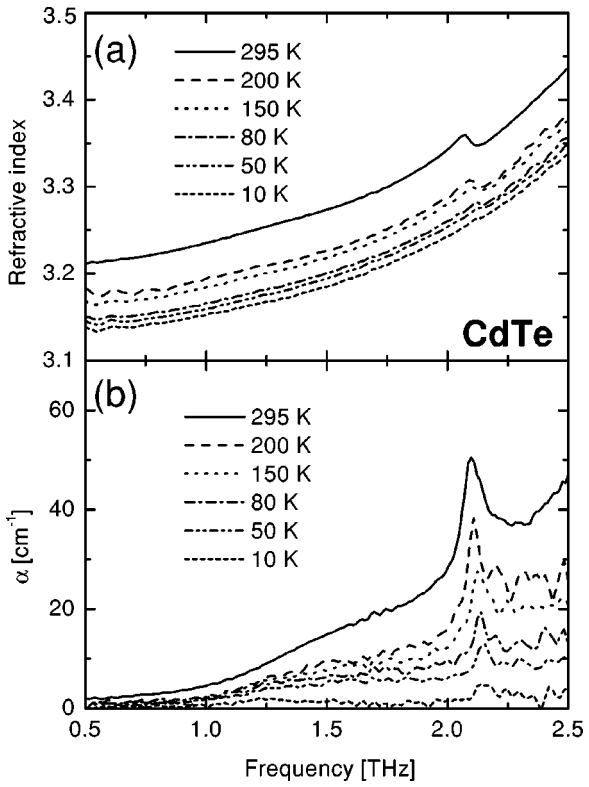

FIG. 2. (a) Index of refraction $n(\nu)$ and (b) absorption coefficient $\alpha(\nu)$ of CdTe from 0.2 to 2.5 THz at temperatures between 10 K and 295 K.

Great care was taken to minimize artifacts caused by different diffraction environments of the sample pulse and the reference pulse upon propagation through the cryostat. The small differences in the propagation characteristics through the sample and reference aperture were measured and explicitly taken into account in the data analysis by correcting subsequent data for the amplitude ratio and phase difference between the empty sample aperture and the reference aperture. This step is of crucial importance for the data analysis due to the small absorption coefficient of the crystal at low temperatures.

The linear-expansion coefficient α_l of CdTe and ZnTe is 5.7×10^{-6} K^{-1} and 8.3×10^{-6} K^{-1}, respectively, at room temperature, and tends to zero at low temperatures.[27,28] Based on these numbers we calculate the contribution from thermal variation of the crystal thickness d to the measured absorption and refractive index changes from 295 K to 10 K to be $\Delta\alpha/\alpha=\Delta n/n<10^{-3}$, which is small enough to be ignored within the signal-to-noise ratio of our data.

III. EXPERIMENTAL SPECTRA

In Fig. 2 we show the index of refraction and absorption coefficient of CdTe at temperatures between 10 K and 295 K, in the frequency range from 0.5 THz to 2.5 THz. At frequencies below 0.5 THz the spectra contain oscillatory features originating from slightly different diffraction environments

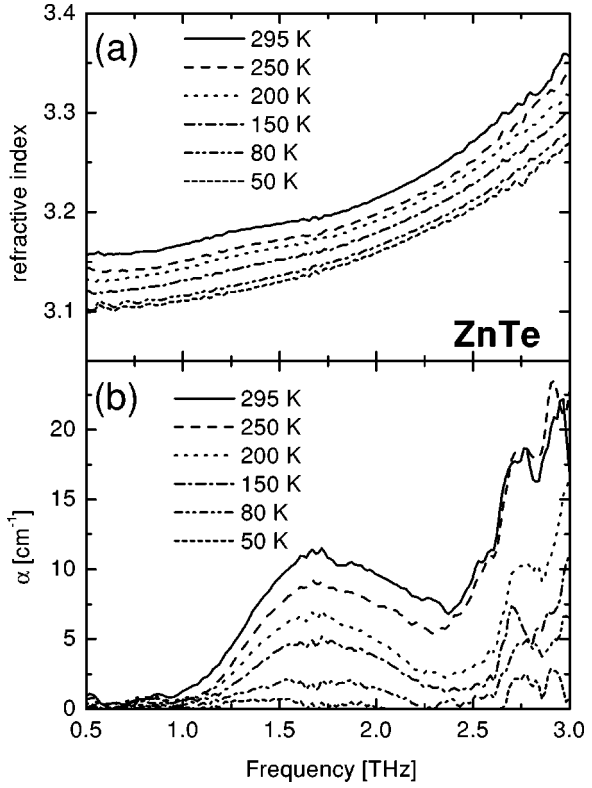

FIG. 3. (a) Index of refraction $n(\nu)$ and (b) absorption coefficient $\alpha(\nu)$ of ZnTe from 0.2 to 3 THz at temperatures between 50 K and 295 K.

of the THz beam upon transmission through the sample and reference apertures, respectively. Apart from these oscillations, no features are observed below 0.5 THz. Both $n(\nu)$ and $\alpha(\nu)$ are gradually increasing at high frequencies. This is due to the low-frequency wing of the TO(Γ) phonon, located at 4.3 THz.[22] The room-temperature dielectric function of CdTe across the fundamental TO resonance has been recorded by Ralph *et al.*,[29] also using THz-TDS.

Superimposed on the low-frequency TO wing a small feature at 2.1 THz is visible both in the index and absorption spectrum. This sharp resonance is known to be the phonon overtone 2TA(X).[21,22] As the temperature of the crystal is lowered, the contribution from the fundamental TO(Γ) phonon becomes less prominent in the absorption spectrum, but remains clearly visible in the index spectrum, where an overall decrease of the value of n is observed. In addition to this effect the 2TA(X) resonance at 2.1 THz decreases in strength, but remains clearly visible in the absorption spectrum even at 10 K, confirming that the resonance is a summation band that remains finite at low temperatures.

In Fig. 3 the index of refraction and absorption coefficient of ZnTe at temperatures between 50 K and 295 K is shown. As in the case of CdTe, the 295-K data a slow increase in both n and α towards high frequencies is observed. This increase is again caused by the TO(Γ) phonon, which in ZnTe is located at 5.32 THz, and additionally by a broad spectral feature centered at 3.7 THz.[15] Additionally, a broad band centered at 1.6 THz is observed on top of the TO(Γ) wing. The origin of these features below the TO(Γ) frequency has so far remained uncertain. Schall *et al.* measured the absorption and index spectra of CdTe and ZnTe at room temperature, and with some uncertainty assigned the 1.6-THz absorption band to the LO(X)-LA(X) mode.[6] In a similar measurement with higher bandwidth, Gallot *et al.* identified the 1.6-THz band with the TA(X) mode and the 3.7-THz band with the LA(X) mode,[15] excitations that are forbidden in pure crystals due to violation of momentum conservation. A fundamental mode away from the Brillouin-zone center could in principle be observed owing to impurity-induced activity,[30] but we find that difference modes must be the origin of both of these bands. Our measurements show that the 1.6-THz band completely disappears at temperatures below 50 K. Combined with the unusual shape of the peak we are therefore led to the assumption that more than one difference mode contribute to this peak.

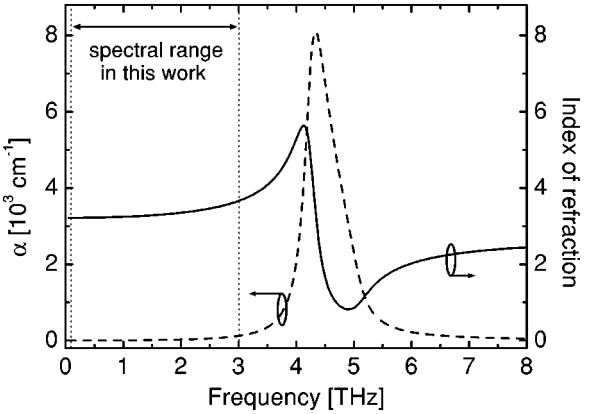

FIG. 4. Absorption coefficient and index of refraction of a Lorentz oscillator with parameters $\nu_{TO}=4.3$ THz, $\gamma_{TO}=0.35$ THz, $\epsilon_{dc}=9.8$, and $\epsilon_{\infty}=6.8$. The region below 3 THz corresponds to the useful experimental bandwidth in the present experiment.

IV. FIRST-ORDER PHONON FEATURES IN THE SPECTRA

We interpret the overall monotonic increase at high frequencies of the index of refraction that is observed both in CdTe and ZnTe in Figs. 2 and 3 as the low-frequency wing of the fundamental-TO phonon resonance. In the case of CdTe, where the TO frequency is 4.3 THz, the slow increase of the absorption coefficient at high frequencies is also attributed to the TO resonance. The shape of a fundamental phonon may be modeled by the expression for a Lorentz oscillator,[31]

$$\epsilon(\nu)=\epsilon_{\infty}+\frac{(\epsilon_{dc}-\epsilon_{\infty})\,\nu_{TO}^2}{\nu_{TO}^2-\nu^2-i\,\gamma_{TO}\nu}, \tag{1}$$

where ν_{TO} is the resonance frequency, γ_{TO} is the width of the resonance (or damping constant), ϵ_{dc} is the static, relative permittivity, and ϵ_{∞} is the permittivity at high frequencies. The difference $\epsilon_{dc}-\epsilon_{\infty}$ is normally referred to as the oscillator strength S. The dielectric function $\epsilon(\nu)$ is related to the index of refraction $n(\nu)$ and absorption coefficient $\alpha(\nu)$ by the relations $\epsilon_r=n^2-\kappa^2$, $\epsilon_i=2n\kappa$, and $\kappa=\alpha c/4\pi\nu$.

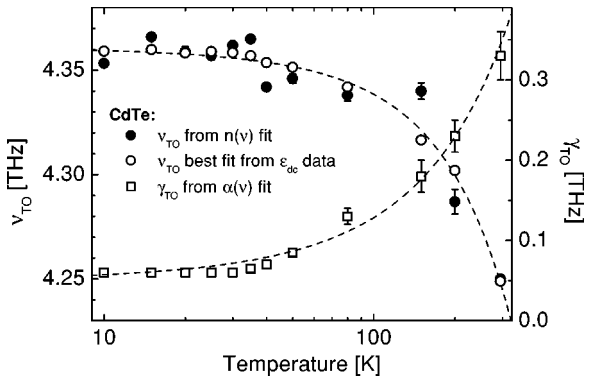

FIG. 5. Temperature dependence of the frequency ν_{TO} and damping rate γ_{TO} of the TO(X) resonance in CdTe. The fit curves are discussed in the text.

In Fig. 4 the absorption coefficient and index of refraction of a Lorentz oscillator is illustrated. The parameters are $\nu_{TO}=4.3$ THz, $\gamma_{TO}=0.35$ THz, $\epsilon_{dc}=9.8$, and $\epsilon_{\infty}=6.8$. As will be described below, these numbers represent room-temperature values of the TO resonance in CdTe. The region below 3 THz indicates the spectral range of the present experiment. Notice that the real and imaginary parts of ϵ are antisymmetric and symmetric around ν_{TO}, respectively, this is not the case for α and n, where a slight asymmetry of both α and n on the high-frequency side of the resonance is visible. This asymmetry becomes more dominant as the damping becomes smaller.

On the low-frequency wing of the resonance frequency ($\nu \ll \nu_{TO}$) the index of refraction and absorption coefficient of a Lorentz oscillator can be approximated by

$$n^2 \approx \epsilon_{\infty} + \frac{(\epsilon_{dc}-\epsilon_{\infty})\,\nu_{TO}^2}{\nu_{TO}^2-\nu^2}, \tag{2}$$

$$\alpha \approx \frac{(\epsilon_{dc}-\epsilon_{\infty})\,\gamma_{TO}\nu^2}{\sqrt{\epsilon_{dc}}c\,\nu_{TO}^2}. \tag{3}$$

These approximations illustrate that while the measured $\alpha(\nu)$ contains information about both ν_{TO} and γ_{TO}, the measured $n(\nu)$ is mainly sensitive to ν_{TO}. Therefore we have used the measured $n(\nu)$ to determine ν_{TO}, and subsequently used the measured $\alpha(\nu)$ to determine γ_{TO}, based on the full dielectric function in Eq. (1). The result of this fitting procedure is shown in Fig. 5, where the temperature dependence of ν_{TO} and γ_{TO} of CdTe is shown.

We find that a second-order polynomial with adjustable coefficients of the form

$$Y(T)=A+B\left(\frac{T}{\theta}\right)+C\left(\frac{T}{\theta}\right)^2, \tag{4}$$

where Y is one of the measured quantities ($\nu_{TO}, \gamma_{TO}, \epsilon_{dc}$), and θ is the characteristic temperature of the phonon, $\theta = h\nu_{TO}/k_B$. For CdTe (ZnTe), $\theta=207(255)$ K.

TABLE I. Coefficients obtained in the fitting procedure of Eq. (4) described in the text.

Parameter	*A*	*B*	*C*	Units
	CdTe ($\theta=207$ K)			
ν_{TO}	4.361	−0.0298	−0.0348	THz
ϵ_{dc}	9.808	0.1719	0.1414	
γ_{TO}/ν_{TO}	0.0116	0.0314	0.0119	THz
	ZnTe ($\theta=255$ K)			
ν_{TO}	5.409	−0.0457	−0.0341	THz
ϵ_{dc}	9.624	0.1583	0.1318	

Jones *et al.*[32] observed a similar temperature behavior of γ_{TO} and ν_{TO} in the alkali halides KBr and AgBr, and Ipatova *et al.*[33] derived an approximate equation describing the ratio γ_{TO}/ν_{TO} in the high-temperature limit ($T>\theta$) for alkali halides with the same functional form as Eq. (4), showing a quadratic variation of the relative linewidth at high temperatures. They demonstrated that cubic and quartic anharmonicities of the potential energy of the crystal give rise to a temperature-dependent width of the fundamental-TO phonon line of the form described by Eq. (4). These cubic and quartic anharmonicity terms correspond to modifications of the line profile caused by three- and four-phonon interactions, respectively. Jones *et al.*[32] described this broadening effect in terms of anharmonicity-induced coupling between different modes of vibration in the crystal, which in the harmonic approximation are completely independent. In the presence of anharmonic forces, energy fed into one resonance may dissipate into other modes, leading to larger damping of the resonance.

The curve shown together with the experimental data for ν_{TO} in Fig. 5 is a fit using Eq. (4), with parameters given in Table I. Using this expression for $\nu_{TO}(T)$, we used the expression given by Ipatova *et al.*[33] to obtain the curve shown together with the experimental data for γ_{TO}. The fitting parameters are again given in Table I. It is clear that the predicted connection between ν_{TO} and γ_{TO} is verified by our experimental data.

The increase of ν_{TO} at low temperatures is connected to the temperature dependence of ϵ_{dc}. This relation can be used to extract the dynamical ionic charge $e_T^{\star}$ of the oscillator. The dynamical ionic charge, or vibrational transition moment $|\langle \partial \mathbf{M}/\partial u \rangle|$, is a measure of the polar character of the vibrational mode. Since the static ionic charge in zincblende structures is close to zero, $e_T^{\star}$ can be attributed to charge redistribution among the atoms. In the case of II-VI zincblende structures the dynamical ionic charge is given by the relation[34,35]

$$e_T^{\star 2}=\frac{4\pi^2\epsilon_0(\epsilon_{dc}-\epsilon_{\infty})\overline{m}V\nu_{TO}^2}{N}, \tag{5}$$

where ϵ_0 is the free-space permittivity, $\overline{m}$ is the reduced mass of the oscillator, and N/V is the number of oscillators

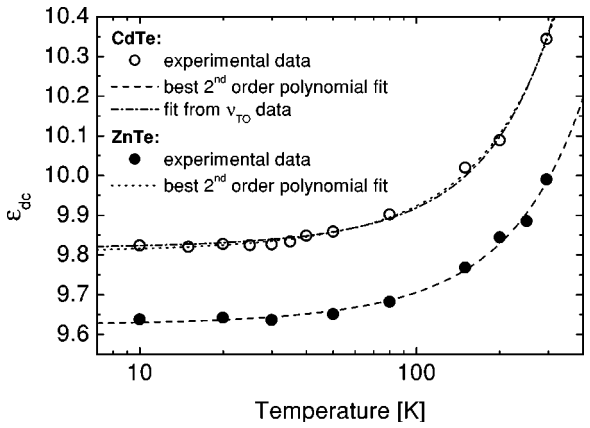

FIG. 6. Experimentally determined temperature dependence of the static permittivity of CdTe (open circles) and ZnTe (full circles). The various fit curves are described in the text.

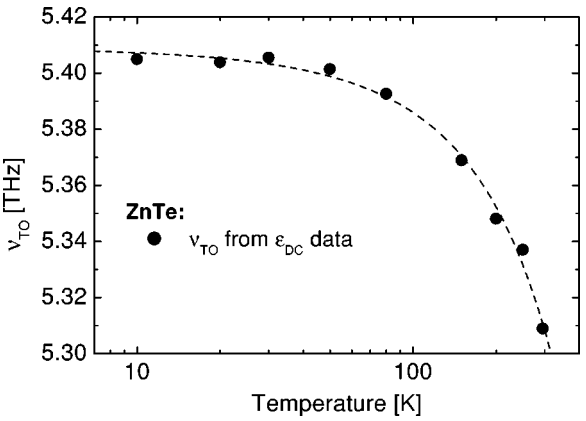

FIG. 7. The TO frequency in ZnTe, calculated from $\epsilon_{dc}(T)$ in Fig. 6. The dashed curve is described in the text.

per volume. With the assumption that the familiar Lyddane-Sachs-Teller relation[36] $\epsilon_{dc}/\epsilon_{\infty}=(\nu_{LO}/\nu_{TO})^2$ is valid within our temperature range, Eq. (5) can be rearranged to

$$\epsilon_{dc}=\frac{e_T^{\star 2}N}{4\pi^2\epsilon_0[1-(\nu_{TO}/\nu_{LO})^2]\overline{m}V}\frac{1}{\nu_{TO}^2}. \tag{6}$$

If both ϵ_{dc} and ν_{TO} is known, then Eq. (6) can be used to determine $e_T^{\star}$.

In Fig. 6 the temperature dependence of the static permittivity ϵ_{dc} of CdTe and ZnTe is plotted. The values are extracted by extrapolation of the index of refraction in Figs. 2 and 3. The result of fitting Eq. (4) to the experimental data is also shown on the graph, and fitting parameters are given in Table I. For CdTe both $\epsilon_{dc}(T)$ and $\nu_{TO}(T)$ is measured, and therefore a fit based on Eq. (6), using parameter values given in Table II, can be performed. The only free parameter is the dynamical ionic charge, and $e_T^{\star}/e=2.28$ gave the best fit, also shown on top of the experimental data for ϵ_{dc} in Fig. 6. Other zincblende crystal structures have dynamical ionic charges in the range $1.8e$–$2.7e$ (Ref. 35).

In the case of ZnTe our data does not permit a statistical meaningful extraction of the temperature dependence of ν_{TO} by fitting of the measured absorption coefficient and index of refraction because of a strong absorption band at 3.7 THz (Ref. 15). At low temperatures this band freezes out, but the TO resonance at 5.32 THz is still at a too-high frequency to allow reliable fitting based on the present data. However, we can use the measured $\epsilon_{dc}(T)$, together with the dynamical ionic charge determined from the room-temperature values of ν_{TO} and ϵ_{dc} to extract $\nu_{TO}(T)$. In Fig. 7 the result of this procedure is shown. The solid circles are calculated from the values of ϵ_{dc} using $e_T^{\star}/e=2.06$, and the dashed curve is a second-order polynomial fit with parameters given in Table I. The data in Figs. 5 and 7 constitute to our best knowledge the first experimental determination of the temperature dependence of ν_{TO} and γ_{TO} in CdTe and ν_{TO} in ZnTe.

The connection between ϵ_{dc} and ν_{TO} can be summarized by the relations $\epsilon_{dc}=K'/\nu_{TO}^2$, and consequently, $\nu_{TO}=\sqrt{K'/\epsilon_{dc}}$. The parameter K' is given in Table II for both CdTe and ZnTe. The data points represented by open circles in Fig. 5 is the calculation of ν_{TO} of CdTe, based on values of ϵ_{dc} shown in Fig. 6.

TABLE II. Parameters for CdTe and ZnTe crystals.

Parameter	**CdTe**	**ZnTe**	Units
N/V	1.47×10^{28} [a]	1.76×10^{28} [a]	m^{-3}
$\nu_{LO,300\ K}$	5.08 [b]	6.25 [b]	THz
$\nu_{TO,300\ K}$	4.20 [b]	5.32 [c]	THz
$\overline{m}$	9.9×10^{-26} [d]	7.2×10^{-26} [d]	kg
$e_T^{\star}/e$	2.28 [e]	2.06 [e]	
K'	186.5 [e]	281.5 [e]	$(THz)^2$

[a]Reference 37.
[b]Reference 39.
[c]Reference 15.
[d]$\overline{m}=(m_1+m_2)/m_1m_2$.
[e]Present work.

V. SECOND-ORDER PHONON FEATURES IN THE SPECTRA

The crystals ZnTe and CdTe crystallize in the cubic zincblende structure [space group $F\bar{4}3m$ (T_d^2)], with four molecular formulas in each unit cell.[37] The critical points in the Brillouin zone are the Γ, X, L, K, and W points. A photon with energy $\hbar\omega$ can interact with phonon modes in a crystal, under the condition that the total energy and momentum of the process is conserved. Energy conservation requires that $\hbar\omega=\Sigma\pm h\nu_i$, where ν_i is the frequency of the individual phonon modes involved in the process. A positive or negative frequency corresponds to the creation or annihilation of a phonon, respectively. Since the momentum of a photon at THz frequencies is much smaller than the momentum of a phonon, momentum conservation is expressed as $\Sigma\pm K_i=0$ for one- and two-phonon processes. This restriction is the reason why one-phonon processes only take place at the center of the Brillouin zone, and the TO(Γ) is the only one-phonon mode in zincblende crystals that couples directly to

the radiation field. Two-phonon processes can occur owing to anharmonicity of the transition moment[38] or of the potential function[31] of the crystal, and occur only if the two phonons originate from the same point in the Brillouin zone, with $K_1=-K_2$ for summation modes and $K_1=K_2$ for difference modes. Although transitions between the phonon branches can occur anywhere in the Brillouin zone, they are most likely to take place at critical points, where the density of states is highest.

At a temperature T the occupation number N of phonons with energy $h\nu$ is given by $N=[\exp(h\nu/kT)-1]^{-1}$. A quantum-mechanical treatment of the interaction between the radiation field with photon number n and phonons gives the probabilities of creation and annihilation of a phonon.[31] The creation probability is

$$P_{N\to N+1}=|\langle\psi_{N+1,n}|H|\psi_{N,n'}\rangle|^2\propto N+1, \tag{7}$$

and the probability of annihilation of a phonon is

$$P_{N\to N-1}=|\langle\psi_{N-1,n}|H|\psi_{N,n'}\rangle|^2\propto N. \tag{8}$$

Here H is the interaction Hamiltonian and ψ is the combined wave function of the phonon and the photon. The probability P_Σ of the creation of two phonons with energies $h\nu_1$ and $h\nu_2$ is calculated by assuming that the two creation events are independent of each other, and taking into account the probability of the reverse process, annihilation of the two phonons. This probability is then $P_\Sigma\propto(N_1+1)(N_2+1)-N_1N_2=1+N_1+N_2$. In a similar manner, the probability P_Δ of the simultaneous creation of one phonon with energy $h\nu_1$ and annihilation of a second phonon with energy $h\nu_2$ ($\nu_1<\nu_2$) is $P_\Delta\propto(N_1+1)N_2-N_1(N_2+1)=N_2-N_1$. Hence it is expected that a summation mode will retain a nonvanishing intensity at low temperatures, whereas a difference mode will disappear from the absorption spectrum at low temperatures with functional forms given by

$$P_\Sigma\propto 1+\frac{1}{\exp(h\nu_1/kT)-1}+\frac{1}{\exp(h\nu_2/kT)-1}, \tag{9}$$

$$P_\Delta\propto \frac{1}{\exp(h\nu_2/kT)-1}-\frac{1}{\exp(h\nu_1/kT)-1}. \tag{10}$$

The magnitude of the functions P_Σ and P_Δ depends on the absolute energy of each of the participating phonon modes and the temperature. Hence the temperature dependence of the absorption band can be used to identify its origin even in the situation where several combinations of phonon-modes match the observed absorption frequency, as is the case in ZnTe.

By taking into account the background absorption and dispersion owing to the TO(Γ) phonon, we can obtain the peak-absorption strength for the additional 1.6-THz and 2.1-THz resonances in ZnTe and CdTe, respectively. These data, normalized to unity at 295 K, are shown in Fig. 8. The error bars in the figure indicate the reproducibility of the data. Together with the experimental data we show the temperature-dependence predicted by Eqs. (9) and (10) with various choices of the fundamental frequencies ν_1 and ν_2, as discussed below.

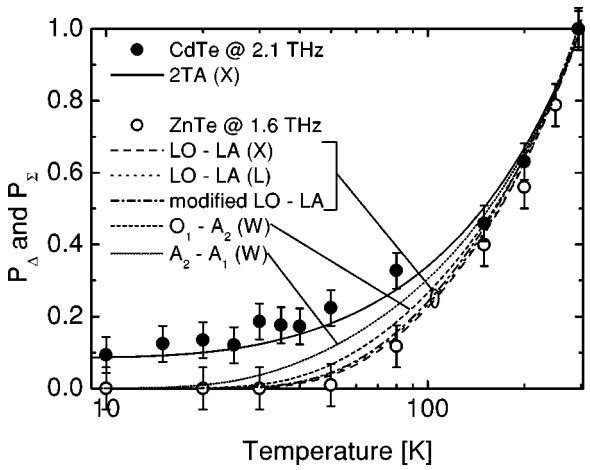

FIG. 8. Temperature dependence of the peak-absorption strength of phonon bands in CdTe and ZnTe together with curves predicted by Eqs. (9) and (10).

In the case of CdTe, we assume that the 2.1-THz feature is the 2TA(X) mode, and use $\nu_1=\nu_2=1.05$ THz (Refs. 21,22) to generate the curve shown as a solid line on top of the experimental data points (solid circles). There is good agreement between the experimentally observed and calculated temperature dependence of the absorption strength, which demonstrates the versatility of the analysis.

In the case of ZnTe, the best agreement between our experimental data and Eq. (10) is obtained for the LO(X)-LA(X) mode and for the LO(L)-LA(L) mode. We use the fundamental frequencies given in the comprehensive work by Ram *et al.*[39] The curves based on these values are shown in Fig. 8 as two-dashed lines together with the experimental data for ZnTe (open circles).

To facilitate the following assignment discussion, the top part of Fig. 9 shows the first Brillouin zone of the fcc lattice, indicating important points of high symmetry. The lower part of Fig. 9 shows a qualitative phonon-dispersion diagram of ZnTe, based on neutron-scattering data given in Ref. 40. Two-phonon processes discussed in the following are indicated by vertical arrows.

The difference modes with a temperature dependence that fits our experimental data, both, have frequencies lower than the observed peak at 1.6 THz. Slight modifications of ν_2 and ν_1 (by -3% and $+10\%$, respectively) in order to obtain a difference of 1.6 THz in the evaluation of Eq. (10) has no influence on the agreement with the experimentally observed temperature dependence. This is illustrated by the dash-dotted curve in Fig. 8, which is calculated with $\nu_2=5.5$ THz, $\nu_1=3.9$ THz, and $\Delta\nu=1.6$ THz. This curve is virtually indistinguishable from the other LO-LA curves shown in the same figure.

The sensitivity of Eq. (10) on the absolute positions of the individual frequencies ν_2 and ν_1 is illustrated by the inclu-

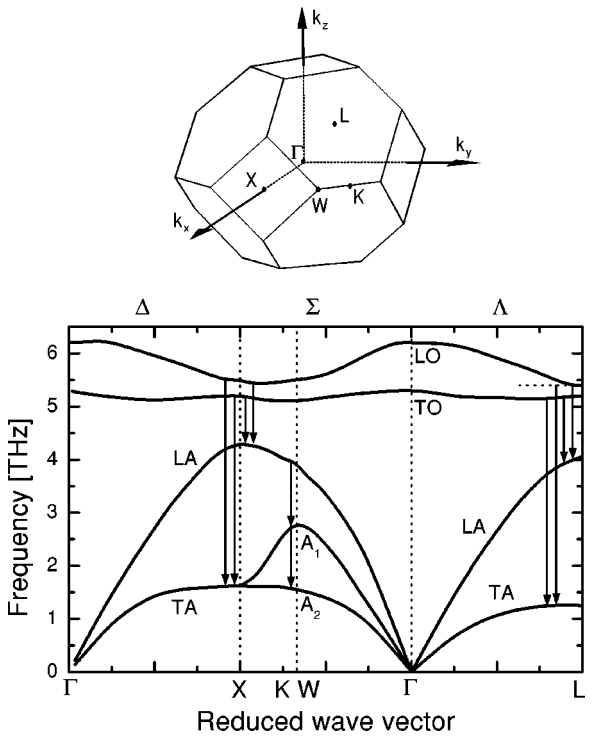

FIG. 9. First Brillouin zone of the fcc lattice indicating positions of high-symmetry points, and phonon dispersion curves of ZnTe, adapted from data given in Ref. 40. Difference phonon modes considered in this work are indicated by vertical arrows.

sion of the alternative assignments $A_1(W)$-$A_1(W)$ and LA(W)-A_1(W), shown as dashed curves in Fig. 8. Judged on the difference frequencies (1.29 THz and 1.35 THz) alone these modes would also be candidates in the assignment. However, since both fundamental frequencies are lower than the LO and LA frequencies, the predicted temperature-dependence does not fit the temperature dependence observed in the experimental data. It is therefore less likely that these modes contribute to the absorption band.

The different infrared-active[41] combination possibilities with difference frequencies near 1.6 THz are summarized in Table III. The resonance frequencies in Table III are adapted from values given by Ram *et al.*[39] except the LO and LA frequencies modified to obtain a difference frequency of 1.6 THz.

It is not possible to find other reasonable two-phonon combinations of fundamental frequencies in the literature that reproduce the 1.6 THz difference frequency. We are therefore led to the conclusion that the 1.6-THz band in ZnTe arises from a mixture of the LO(X)-LA(X) and LO(L)-LA(L) combination modes, and we note that the experimental results presented here and in Refs. 6 and 15 may be used to improve accuracy in the determination of the fundamental phonon frequencies.

The increasing absorption above the 1.6-THz band in ZnTe is the low-frequency wing of the 3.7-THz feature observed by Gallot *et al.*[15] This wing disappears as the temperature is lowered, but the limited signal-to-noise ratio at high frequencies in our data does not allow a closer analysis. The present data, however, indicate that this band also originates from difference modes, and we suggest that the 3.7-THz band is a superposition of the infrared-active[41] TO(X)-TA(X), TO(L)-TA(L), LO(X)-TA(X), and LO(L)-TA(L) difference processes. The frequencies of these modes fall between 3.6 and 4.1 THz,[39] and are summarized in Table III.

TABLE III. Phonon frequencies and their difference combinations in ZnTe, adapted from values given by Ram *et al.*[39]

Mode:	ν_2 (THz)	ν_1 (THz)	$\Delta\nu$ (THz)
1.6-THz band assignment			
LO(X)-LA(X)	5.53	4.29	1.24
LO(L)-LA(L)	5.35	4.29	1.06
LO-LA (modified)	5.50	3.90	1.60
$A_1(W)$-$A_2(W)$	3.06	1.77	1.29
LA(W)-A_1(W)	4.41	3.06	1.35
3.7-THz band assignment			
TO(X)-TA(X)	5.23	1.62	3.61
TO(L)-TA(L)	5.17	1.29	3.88
LO(X)-TA(X)	5.53	1.62	3.91
LO(L)-TA(L)	5.35	1.29	4.06

VI. CONCLUSION

We have measured the temperature-dependent absorption- and refractive-index spectra of CdTe and ZnTe between 10 K and 295 K and shown that at temperatures below 80 K ZnTe becomes virtually transparent below the TO(Γ) frequency. The freeze out of all absorption bands enables higher detection efficiency and bandwidth for THz pulses in ZnTe. Recently we demonstrated a more than threefold increase of the detection efficiency at 80 K compared to operation at room temperature at frequencies above 3 THz in a 250-μm thick crystal.[42]

The experimentally obtained absorption and dispersion spectra of CdTe and ZnTe have been shown to contain important information about the temperature dependence of the fundamental TO(Γ) resonance in both crystals. We have assigned the absorption band in ZnTe at 1.6 THz to a mixture of LO(X)-LA(X) and LO(L)-LA(L) modes, and demonstrated that the 3.7-THz absorption band also originates from a combination of difference modes.

As the clock rate of electronic circuits progresses toward THz frequencies, the need for ultrafast opto-electronic components with low-loss and well-understood dispersion becomes urgent. Our results show that ZnTe, operated at the temperature of liquid nitrogen, is a promising compound material for devices with extremely high bandwidth well into the THz regime.

ACKNOWLEDGMENT

This work was supported by the Deutsche Forschungsgemeinschaft, under Project No. SFB 276, TP C14.

[1] Q. Wu and X.-C. Zhang, Appl. Phys. Lett. **67**, 3523 (1995).
[2] A. Nahata, D.H. Auston, T.F. Heinz, and C. Wu, Appl. Phys. Lett. **68**, 150 (1996).
[3] P. Uhd Jepsen, C. Winnewisser, M. Schall, V. Schyja, S.R. Keiding, and H. Helm, Phys. Rev. E **53**, 3052 (1996).
[4] H. Harde, N. Katzenellenbogen, and D. Grischkowsky, J. Opt. Soc. Am. B **11**, 1018 (1994).
[5] C. Rønne, P.-O. Åstrand, and S.R. Keiding, Phys. Rev. Lett. **82**, 2888 (1999).
[6] M. Schall, H. Helm, and S.R. Keiding, Int. J. Infrared Millim. Waves **20**, 595 (1999).
[7] B.I. Greene, P.N. Saeta, D.R. Dykaar, S. Schmitt-Rink, and S.L. Chuang, IEEE J. Quantum Electron. **28**, 2302 (1992).
[8] R. McElroy and K. Wynne, Phys. Rev. Lett. **79**, 3078 (1997).
[9] M. Schall and P. Uhd Jepsen, Opt. Lett. **25**, 13 (2000).
[10] E. Knoesel, M. Bonn, J. Shan, and T.F. Heinz, Phys. Rev. Lett. **86**, 340 (2001).
[11] R.H.M. Groeneveld and D. Grischkowsky, J. Opt. Soc. Am. B **11**, 2502 (1994).
[12] J. Zielbauer and M. Wegener, Appl. Phys. Lett. **68**, 1223 (1996).
[13] H.J. Bakker, G.C. Cho, H. Kurz, Q. Wu, and X.-C. Zhang, J. Opt. Soc. Am. B **15**, 1795 (1998).
[14] G. Gallot and D. Grischkowsky, J. Opt. Soc. Am. B **16**, 1204 (1999).
[15] G. Gallot, J. Zhang, R.W. McGowan, T.-I. Jeon, and D. Grischkowsky, Appl. Phys. Lett. **74**, 3450 (1999).
[16] P.Y. Han and X.-C. Zhang, Appl. Phys. Lett. **73**, 3049 (1998).
[17] A. Leitenstorfer, S. Hunsche, J. Shah, M.C. Nuss, and W.H. Knox, Appl. Phys. Lett. **74**, 1516 (1999).
[18] G.C. Cho, P.Y. Han, X.-C. Zhang, and H.J. Bakker, Opt. Lett. **25**, 1609 (2000).
[19] A. Leitenstorfer, S. Hunsche, J. Shah, M.C. Nuss, and W.H. Knox, Phys. Rev. Lett. **82**, 5140 (1999).
[20] A. Leitenstorfer, S. Hunsche, J. Shah, M.C. Nuss, and W.H. Knox, Phys. Rev. B **61**, 16 642 (2000).
[21] O.M. Stafsudd, F.A. Haak, and K. Radisavljević, J. Opt. Soc. Am. **57**, 1475 (1967).
[22] G.L. Bottger and A.L. Geddes, J. Chem. Phys. **47**, 4858 (1967).
[23] R.E. Nahory and H.Y. Fan, Phys. Rev. **156**, 825 (1967).
[24] A. Bartels, T. Dekorsy, and H. Kurz, Phys. Rev. Lett. **84**, 2981 (2000).
[25] S.E. Ralph and D. Grischkowsky, Appl. Phys. Lett. **59**, 1972 (1991).
[26] M. Walther, Diploma thesis, University of Freiburg, 2000.
[27] J.F. Vetelino, S.S. Mitra, and K.V. Namjoshi, Phys. Rev. B **2**, 967 (1970).
[28] D.N. Talwar, M. Vandevyver, K. Kunc, and M. Zigone, Phys. Rev. B **24**, 741 (1981).
[29] S.E. Ralph, S. Perkowitz, N. Katzenellenbogen, and D. Grischkowsky, J. Opt. Soc. Am. B **11**, 2528 (1994).
[30] G.A. Slack and S. Roberts, Phys. Rev. B **3**, 2613 (1971).
[31] K. D. Moeller and W. G. Rothschild, *Far-Infrared Spectroscopy* (Wiley, New York, 1971), Chap. 12.
[32] G.O. Jones, D.H. Martin, P.A. Mawer, and C.H. Perry, Proc. R. Soc. London, Ser. A **261**, 10 (1961).
[33] I.P. Ipatova, A.A. Maradudin, and R.F. Wallis, Phys. Rev. **155**, 882 (1967).
[34] E. Burstein, J. Phys. Chem. Solids Suppl. **1**, 315 (1965).
[35] E. Burstein, M.H. Brodsky, and G. Lucovsky, Int. J. Quantum Chem. **1S**, 759 (1967).
[36] R.H. Lyddane, R.G. Sachs, and E. Teller, Phys. Rev. **59**, 673 (1941).
[37] *Handbook of Optics*, edited by E. W. van Stryland, D. R. Williams, W. L. Wolfe, and M. Bass (McGraw-Hill, New York, 1995), Vol. II, Chap. 33.
[38] M. Lax and E. Burstein, Phys. Rev. **97**, 39 (1955).
[39] R.K. Ram, S.S. Kushwaha, and J.S. Rajput, J. Phys. Soc. Jpn. **58**, 4032 (1989).
[40] N. Vagelatos, D. Wehe, and J.S. King, J. Chem. Phys. **60**, 3613 (1974).
[41] J.L. Birman, Phys. Rev. **131**, 1489 (1963).
[42] M. Schall and P. Uhd Jepsen, Appl. Phys. Lett. **77**, 2801 (2000).